

**Atomistic simulation study of the shear-band deformation mechanism in Mg-Cu metallic glasses**Nicholas P. Bailey,<sup>1,\*</sup> Jakob Schiøtz,<sup>2</sup> and Karsten W. Jacobsen<sup>1</sup><sup>1</sup>*CAMP, NanoDTU, Department of Physics, Technical University of Denmark, 2800 Lyngby, Denmark*<sup>2</sup>*Danish National Research Foundation's Center for Individual Nanoparticle Functionality, CINF, NanoDTU, Department of Physics, Technical University of Denmark, 2800 Lyngby, Denmark*

(Received 12 September 2005; revised manuscript received 23 November 2005; published 14 February 2006)

We have simulated plastic deformation of a model Mg-Cu metallic glass in order to study shear banding. In uniaxial tension, we find a necking instability occurs rather than shear banding. We can force the latter to occur by deforming in plane strain, forbidding the change of length in one of the transverse directions. Furthermore, in most of the simulations a notch is used to initiate shear bands, which lie at a 45° angle to the tensile loading direction. The shear bands are characterized by the Falk and Langer local measure of plastic deformation  $D_{\min}^2$ , averaged here over volumes containing many atoms. The  $D_{\min}^2$  profile has a peak whose width is around 10 nm; this width is largely independent of the strain rate. Most of the simulations were, at least nominally, at 100 K, about  $T_g/3$  for this system. The development of the shear bands takes a few tens of ps, once plastic flow has started, more or less independent of strain rate. The shear bands can also be characterized using a correlation function defined in terms of  $D_{\min}^2$ , which, moreover, can detect incipient shear bands in cases where they do not fully form. By averaging the kinetic energy over small regions, the local temperature can be calculated, and this is seen to be higher in the shear bands by about 50–100 K. Increases in temperature appear to initiate from interactions of the shear bands with the free surfaces and with each other, and are delayed somewhat with respect to the localization of plastic flow itself. We observe a slight decrease in density, up to 1%, within the shear band, which is consistent with notions of increased free volume or disorder within a plastically deforming amorphous material.

DOI: [10.1103/PhysRevB.73.064108](https://doi.org/10.1103/PhysRevB.73.064108)

PACS number(s): 62.20.Fe, 81.05.Kf

**I. INTRODUCTION**

The mechanical properties of bulk metallic glasses<sup>1,2</sup> (BMGs) are the subject of intense research. A host of applications is envisaged if only reasonable macroscopic plasticity could be achieved, rather than the intense localization into shear bands which typically occurs.<sup>3</sup> In, for example, a uniaxial tension or compression test, failure occurs when a single shear band crosses the entire sample, with less than 1% macroscopic ductility. Recently reported exceptions include a Pt-based BMG<sup>4</sup> and a Cu-Zr BMG,<sup>5</sup> both of which exhibited 20% plastic deformation (in compression) before failure. Ideas for enhancing ductility are based mainly on creating BMG composites, which incorporate nanosized crystalline particles in an amorphous matrix,<sup>6</sup> the idea being to interfere with the development and propagation of shear bands. Leaving aside development, propagation and interactions, there is still much to be understood about the properties of individual shear bands. It is not clear, for example, what kind of structural changes occur within a shear band—which would give rise, for example, to the contrast observed in TEM measurements. It is hoped that atomistic simulation could shed light on the nature of shear bands, but the observation of even one shear band has been limited to a few cases;<sup>7–10</sup> these typically involve simplified model systems involving rigid walls, two-dimensional materials, or pairwise interatomic potentials that have certain limitations regarding the mechanical properties of metals.<sup>11,12</sup> In this article we report observation of shear bands and calculation of characteristic features in simulations of a realistic model of an amorphous alloy deformed in tension.

The atomistic simulation of deformation in amorphous materials has mostly dealt with rather small systems of a few

thousands or tens of thousands of atoms.<sup>7,8,13,14</sup> Such numbers correspond to length scales of at most a few nanometers, although this can be increased by making purely two-dimensional simulations.<sup>8</sup> Studies of the fracture surfaces of BMGs (deformed until failure by shear band propagation) show feature sizes of the order of one micron.<sup>5,15</sup> If this length scale was representative of the thickness of a shear band, one might suspect them not to be observable in simulation, even with system sizes as large as  $10^9$  atoms (around the size of the largest simulations of material deformation<sup>16–18</sup>). TEM studies<sup>19,20</sup> of deformed (B)MGs have, however, shown that the thicknesses of shear bands that are not involved in the ultimate sample failure are rather smaller, some 10–60 nm. The lower limit is well within the range of atomistic simulation. Already in 1993, Mott *et al.*,<sup>21</sup> using simulations with sizes of only a few nm, were able to infer a length scale for inhomogeneous flow of 10 nm, which gives hope to the idea that inhomogeneity on this length scale could be observed.

**II. SIMULATIONS****A. Potential, obtaining glassy configurations**

The material we simulate is  $\text{Mg}_{0.85}\text{Cu}_{0.15}$ , which is the optimal glass-forming composition for the Mg-Cu system.<sup>22</sup> This system is interesting because the addition of a small amount of Y makes it a BMG with high strength and low weight.<sup>23</sup> The interatomic potential is the effective medium theory,<sup>24</sup> fitted to properties of the pure elements and intermetallic compounds obtained from experiment and density functional theory calculations. Glassy configurations were created by cooling from a liquid state above the melting

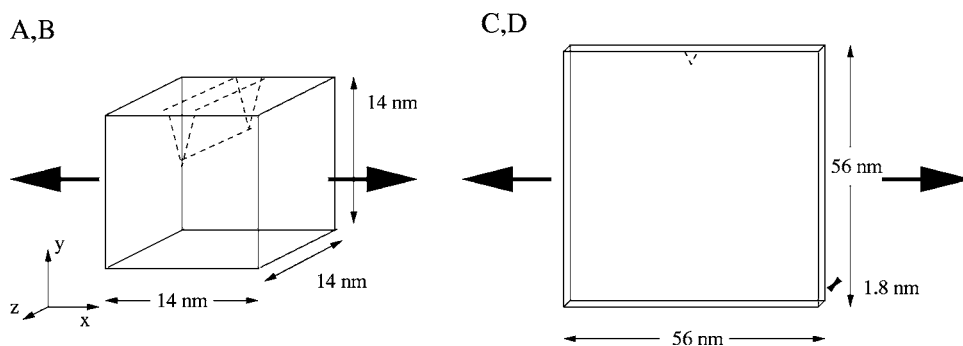


FIG. 1. Schematic diagrams of the main geometries used. B and D have notches while A and C do not. The large arrows indicate the direction of applied strain.

temperature down to  $T=0$ , using constant temperature and pressure molecular dynamics (MD). The temperature was stepped down 35 K at a time; MD was run at each temperature for 130 ps, giving an overall effective cooling rate of 0.72 K/ps. Periodic boundary conditions (PBC) were employed in the cooling process. For each temperature during cooling, thermodynamic averages of the enthalpy were recorded. The numerical derivative of these, the specific heat, shows a clear signature of the glass transition, namely a jump of around 300–350 K ( $=T_g$ , the glass transition temperature). Further details of the potential, the method for creating the zero-temperature glassy configurations, and the determination of  $T_g$  may be found in Ref. 25. We have calculated the elastic constants of the resulting glass and find that the shear and bulk moduli are  $G=7.8$  GPa and  $B=41$  GPa, respectively, at zero temperature. We note that their ratio,  $G/B=0.19$ , indicates that this is a fairly ductile material, according to the criterion of Lewandowski *et al.*<sup>26</sup> (this ratio corresponds to a relatively high Poisson ratio of 0.41).

### B. Geometry

Three basic sample geometries were used:  $14 \times 14 \times 14$  nm,  $56 \times 56 \times 1.8$  nm, and  $28 \times 28 \times 14$  nm, containing  $1-5 \times 10^5$  atoms (see Table I). These were generated from their own cooling runs. In addition, two samples (G and H) were generated by periodically repeating the  $56 \times 56 \times 1.8$  nm sample in the  $x$  and  $y$  directions, respectively. Having samples that are thin in the  $z$  direction, as in samples C-H, allows relatively large extents in the  $x$  and  $y$  directions for a given number of atoms. We have not observed very

TABLE I. Parameters of the different sample geometries.  $N$  indicates the number of atoms, while UT and PS stand for uniaxial tension and plane strain, respectively.

Label	Dimensions (nm)	$N$	Notch depth	Loading
A	$14 \times 14 \times 14$	131 072	0	UT
B	$14 \times 14 \times 14$	128 197	4	UT
C	$56 \times 56 \times 1.8$	262 144	0	PS
D	$56 \times 56 \times 1.8$	261 619	6	PS
E	$28 \times 28 \times 14$	519 565	4	PS
F	$56 \times 56 \times 1.8$	260 035	12	PS
G	$112 \times 56 \times 1.8$	523 768	6	PS
H	$56 \times 112 \times 1.8$	523 761	6	PS

different behavior as a function of the  $z$  thickness.

In order to generate shear bands more readily at high strain rates, we have introduced in some cases a notch on the free surface with normal in the positive  $y$  direction. The depth of the notch is 4–12 nm (Table I) and the opening angle  $20^\circ$ . Presumably much larger imperfections are present on the surfaces of experimental specimens. Two sample geometries are shown in Fig. 1, while Table I lists all of the samples used in this work.

### C. Deformation

All deformation simulations presented here involve straining in the  $x$  direction, in which periodic boundary conditions (PBC) are maintained, at a constant strain rate. Our first simulations had free surfaces in the  $y$  and  $z$  directions; the loading mode is thus “uniaxial tension.” As we discuss later, this geometry leads to a necking, rather than shear-banding, instability. To encourage the latter, in our second, larger, set of simulations, we have applied PBC to the  $z$  direction, and fixed the length in this direction. This is equivalent to enforcing “plane-strain” deformation and is found to suppress the necking instability in favor of a shear-banding one.

For deformation runs, the system was evolved using a Nosé–Hoover thermostat;<sup>27</sup> a constant strain rate was maintained by an appropriate rescaling of atomic coordinates every time step prior to letting them move according to the potential forces. The time step used was 2 fs. Two strain rates were used: the “faster rate”  $2.4 \times 10^9$  s<sup>-1</sup> and the “slower rate”  $2.0 \times 10^8$  s<sup>-1</sup>. In all simulations the velocities (the rate of change of length) are considerably below the speed of sound (by a factor of 40 for the faster rate); thus, there is plenty of time for the influence of relaxations and transformations to travel to other parts of the material. The strain rate is still relatively high compared to the damping time for the lowest vibrational modes of the system, however, and this shows up as an oscillation in the stress, with a period corresponding to a standing wave oriented perpendicular to the loading direction. This can be reduced, but not eliminated, by applying rescaling also in the directions that had free surfaces ( $y$  and  $z$  for uniaxial deformation,  $y$  only for plane strain), using an effective Poisson ratio  $\nu$ . We use  $\nu=0.5(1)$ , which tends to conserve volume in three- (two-) dimensional deformation; this is appropriate for the plastic flow regime, but not for the initial elastic phase; hence stress oscillations are still apparent at the faster strain rate.

### D. Thermostat issues

For almost all simulations, the temperature was set to 100 K. Since the glass transition itself is around room tem-

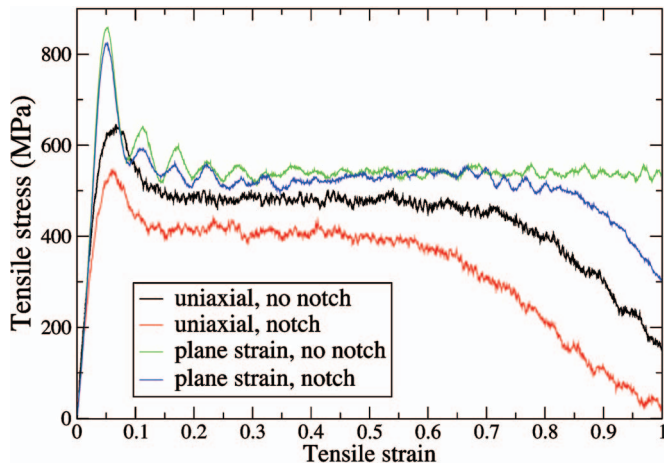


FIG. 2. (Color) Stress-strain curves for samples A, B, C, and D deformed at the faster strain rate.

perature, one would expect homogeneous deformation at that temperature, and it is necessary to go somewhat lower in temperature to be able to simulate inhomogeneous deformation.

Because the goal of these simulations was to study localization phenomena, and because these phenomena have also been associated with localized heating (local temperature increases; see below), it is worth considering the effect of the thermostat. As a system is deformed it will heat up; the question is then how heat can leave the system. In a real system it leaves via the boundaries, a process involving length and time scales much greater than those accessible to simulations. Simulation thermostats, such as Nosé-Hoover, necessarily accelerate in an artificial way the removal of heat; in this case a quantity that looks like an effective friction (but that can become negative) is varied dynamically so as to maintain a set average temperature. When the deformation processes favor a local increase of temperature, the thermostat compensates by tending to reduce the temperature everywhere: away from the locally heated part of the system this means below the nominal temperature, which is clearly unphysical. Possible improvements could be to use a Langevin thermostat<sup>27</sup> instead, which allows local equilibration to take place in a hot spot without anything different taking place away from the spot, or a thermostat that acts only on atoms within a “boundary region” far away from the region of interest. We have not done this—there would still be questions about the realism of these schemes—but to check for effects

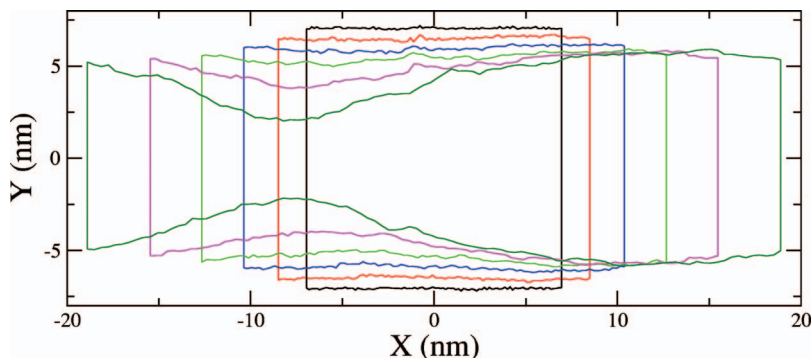


FIG. 3. (Color) Outline of sample A deformed in uniaxial tension after 0%, 20%, 40%, 60%, 80%, and 100% strain.

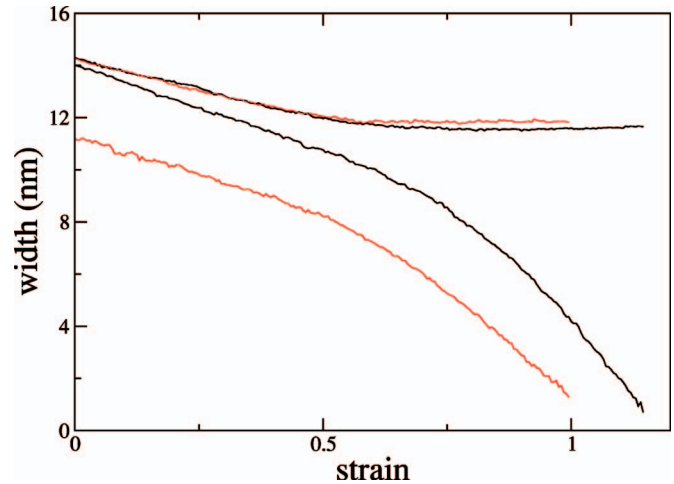


FIG. 4. (Color) Minimum and maximum widths in the  $y$  direction, for samples A (black) and B (red) deformed in uniaxial tension, as a function of strain.

associated with the thermostat, in some simulations the thermostat was turned off after an initial equilibration; thus the dynamics was ordinary Newtonian, plus the imposed strain rate. Note that when the thermostat was on, the internal kinetic energy used to determine how close the system is to the desired temperature is computed not from the actual velocities, but from “internal” velocities that do not include the homogeneous part associated with the strain rate.

### III. NECKING VERSUS SHEAR-BANDING INSTABILITY

Our first simulations strained samples A and B (with/without a notch) in uniaxial tension, that is, with free surfaces on the sides perpendicular to the strain direction, and the faster strain rate. The stress-strain curves are shown in Fig. 2 as the two lower curves. The initial peak does not necessarily represent an instability, since this is a strain-controlled simulation, but it does mark the point beyond which a localization instability may take place. In the sample without a notch (A), the stress stays relatively constant for a while, during which there is homogeneous deformation, until a noticeable drop begins, around 70%. This marks the necking instability. In sample B (notched) the instability appears to occur sooner, around 60% strain.

Since the stress plotted in these figures represents an average over the whole system, and the stress field is not ho-

mogeneous once necking starts, a better indication of the onset of necking might be found by studying the geometrical changes quantitatively. Outlines of sample A, projected onto the  $xy$  plane, at various degrees of deformation, are shown in Fig. 3. The necking starts as a perturbation with wavelength similar to the periodic length in the  $x$  direction. In Fig. 4 we show the maximum and minimum values, with respect to  $x$ , of the widths, as a function of strain, for samples A and B. The quantity that shows the most distinct change is the maximum width, which in both simulations stops decreasing fairly abruptly around 60% strain. The minimum width only shows a gradual change in slope.

We have seen this necking instability also at slower strain rates, at different temperatures, and with different configurations of the notch. This is a little surprising because experimentally, shear banding invariably occurs before necking. The disparity presumably comes from the local nature of a shear band compared with the “global” nature of a necking instability, which takes much longer to grow than the localized shear band. In a macroscopic sample the effective “wavelength” of the necking mode will be of order of the sample width, while the characteristic size of a shear band is still on the order of tens of nm, making the latter much more likely to win the competition of instabilities. Such a large difference in scales is not present in the simulations. Another factor that slows down the shear-banding instability relative to necking in the simulation is the necessity of breaking symmetry in order to choose the orientation of the shear plane.

In order to suppress the necking instability so that we could study shear bands, we adopted the two-dimensional, plane-strain, mode of loading described above. This breaks the symmetry and allows shear bands to form, rather than a neck. We start by considering sample D, which has a notch. A first simple way to visualize the deformation may be termed “stripe-painting,” because one can think of it as taking a paintbrush dipped in black paint, and painting stripes on the sample before deformation. Taking the undeformed configuration, all atoms are binned according to their  $y$  position, and those in odd bins are labeled “black.” This designation is maintained throughout the deformation, and in visualizing any later configuration, only the black atoms are shown. A similar method was used recently by Shimokawa *et al.*<sup>28</sup> Figure 5 shows how the initial straight, parallel stripes become stretched as the deformation proceeds. It is clear that most of the deformation takes place in two bands that lead away from the notch at  $45^\circ$ , while little deformation takes place in the remaining material. After around 80% strain the shear band on the left takes over completely and transforms into a mode resembling necking, which eventually leads to the complete failure of the sample.

In the absence of a notch, and at the faster strain rate, no localization occurs until an extreme amount of deformation has taken place. Using the method outlined below to identify plastically deforming regions, sporadic “hot spots” of plasticity are observed, but these do not coalesce into a shear band. The sample deforms more or less homogeneously until well over 100% strain, when a kind of two-dimensional necking occurs and causes ultimate failure. At a slower strain rate a sustained shear band does appear. This will be discussed more below.

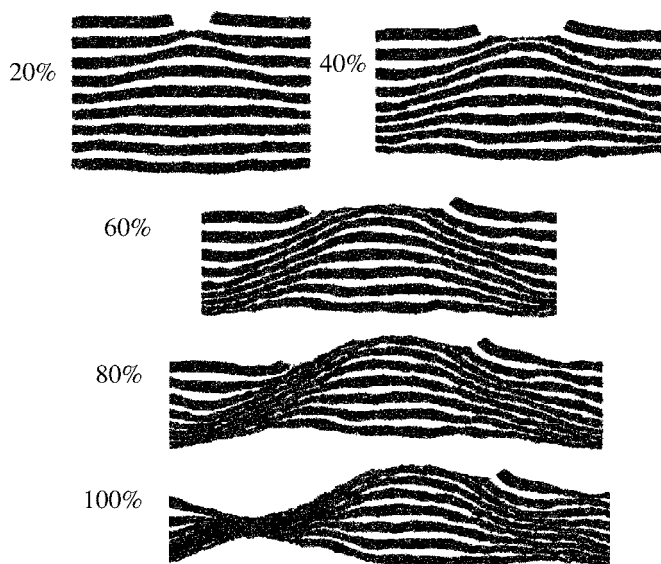


FIG. 5. Visualization by stripe painting in sample D deformed at the faster strain rate, at different amounts of strain.

#### IV. QUANTIFYING SHEAR BANDS

In order to demonstrate the localization of shear more explicitly, we use the technique introduced by Falk and Langer,<sup>13</sup> which for a given pair of configurations in the deformation history, assigns to every atom a number,  $D_{min}^2$ .  $D_{min}^2$  quantifies to what extent changes in the local environment of the atom (characterized by the displacement vectors of its nearest neighbors), from one configuration to another, can be described by an affine transformation (a strain matrix). Specifically  $D_{min}^2$  represents the residual displacement differences unaccounted for by the best-fit strain matrix for that atom. The procedure also yields, of course, this matrix, but we do not use it here. We use configurations differing in global strain by 0.5% at all times. With this quantity defined for all atoms, we can use it in two ways: First by visualizing the atoms, showing only those with  $D_{min}^2$  above a certain cutoff value ( $10 \text{ \AA}^2$ ); second, by doing a coarse graining of the system—dividing it into boxes within which the average  $D_{min}^2$  is computed, called  $D_{ave}^2$ . The advantage of the first method is that one can see dramatically the actual plastic processes and how they are confined in the main to particular regions of space; that of the second is that information from all atoms is used, and there is no arbitrary cutoff.

Figure 6 shows clear shear bands from 10% strain and after. Even at 5% strain there is a noticeable sign of the emerging shear bands. Because the sample is initially square, the shear bands first hit the periodic boundaries at points about halfway across the sample. As the sample elongates and narrows, these points approach the far boundary. In the meantime, each shear band can be seen intersecting with the periodic image of the other one. Eventually (not shown), the shear bands completely separate from each other. Subsequently one of the shear bands becomes dominant and leads to ultimate failure by a shearing off process that in its final stages resembles necking. It might be supposed that there could be artifacts due to the intersection of the bands. We

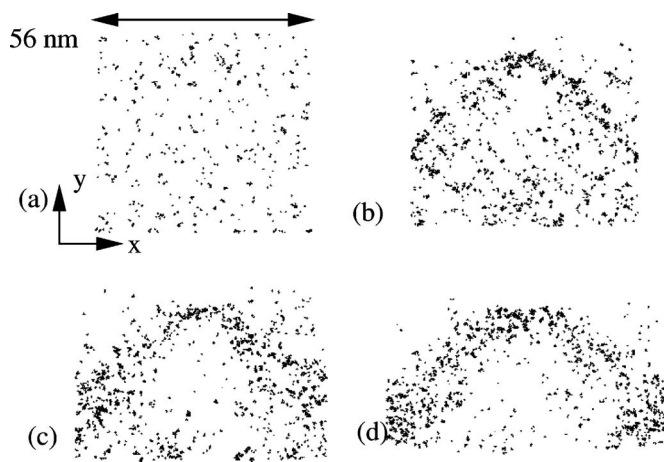


FIG. 6. Shear bands visualized using  $D_{min}^2$  in sample D deformed at the faster strain rate, at (a) 5%, (b) 10%, (c) 20%, and (d) 30% strain.

have carried out a simulation twice as long in the  $x$  direction in order to check for these. Little difference was seen; in particular, the stress-strain curves are almost identical. A visualization of the temperature of the extra-long simulation is shown later in the paper.

Figure 7 shows profiles of  $D_{ave}^2$  for samples D and E deformed at the fast rate, at strain 5% and 10%. Profiles taken at different points along the shear band are shown; the points are identified by their  $y'$  value, where the  $x', y'$  coordinate system is defined in the inset. Each point in a profile represents an average over a box containing a few thousand atoms; wider boxes are chosen in the case of sample D because of the thinness in the  $z$ -direction. There is some noise in the data, particularly for sample D, but we can note the following: The band is barely present at 5% strain but develops fully between 5% and 10% strain, that is, between 20 and

40 ps after the start of deformation. This occurs the whole way along its length, as least as far as the intersection point with the other band, although the part closest to the notch grows a little faster. The widths for sample D are around 10 nm, while the smoother profiles for sample E are somewhat smaller and narrower, with widths around 8 nm.

We now consider simulations at the slower strain rate. The stress-strain curve for sample D is compared in Fig. 8 with those at the faster strain rate. The peak and flow stresses are reduced, as is to be expected. The stress oscillations are greatly reduced in amplitude and period (the latter in proportion to the reduction in strain rate). From the visualizations in Fig. 9 we see immediately that the shear bands are clearly developed at a much smaller strain, already at 5%. In fact, most of the development seems to take place from 4% to 5% strain, which corresponds to a time of 50 ps, of the same order as the 20 ps from the higher strain rate. As the strain approaches 10% the right-hand band becomes much more intense than the left, and presumably dominates the deformation. It is not clear what the mechanism for such a selection might be. The intensity, measured by the height of the  $D_{ave}^2$  profile (not shown) is also greater than that for the faster strain rate. The widths are again in the range 8–10 nm.

In order to check for artifacts associated with the thermostat, we have run some simulations with the thermostat turned off at the beginning of deformation. Stress-strain curves for both strain rates are shown in Fig. 8, where the main effect is a gradual reduction of flow stress as the system heats up. There are no major differences in the  $D_{ave}^2$  profiles. Simulations were also done on a similar geometry, differing only in that the notch had a depth of 12 nm instead of 6 nm, and on the standard notched sample, but at a lower temperature of 50 K. The faster strain rate was used in these cases. Again, there is not much difference. At 10% strain the shear band width is only 5 nm compared to 7 nm for the 100 K deformation. At 20% strain it is 9–10 nm (away from the notch) compared to 11–13 nm.

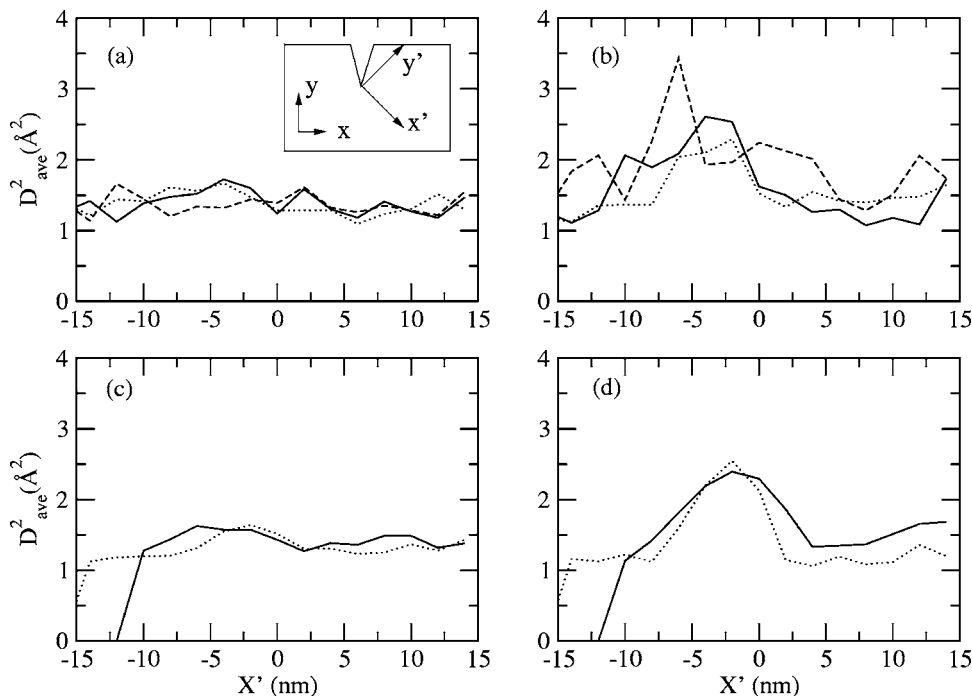


FIG. 7. Profiles of  $D_{ave}^2$  from samples (a) D at 5%, (b) D at 10%, (c) E at 5%, (d) E at 10% strain, deformed at the “faster” strain rate. Solid, dotted, and dashed lines are for  $y'$  centered on  $-10$ ,  $-20$ , and  $-30$  nm, respectively, for sample D. Solid, dotted lines are for  $y'$  centered on  $-9$  and  $-13$  nm, respectively, for sample E (note here that the data fall to zero at negative  $x'$  corresponding to the edge of the sample).

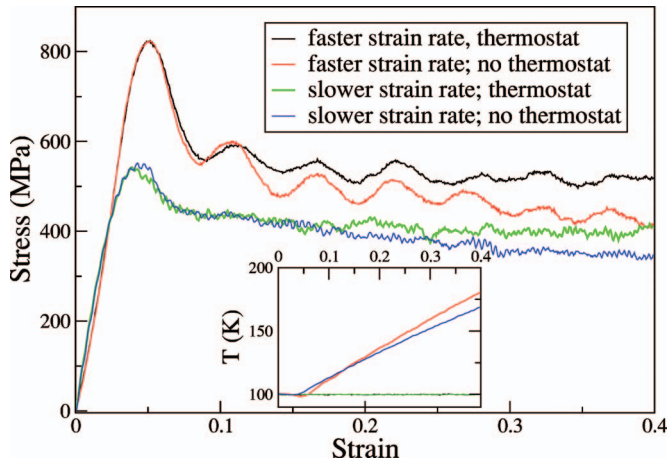


FIG. 8. (Color) Stress-strain curves compared for different strain rates, and with/without thermostat, for sample D. The inset shows the temperature, determined from the average kinetic energy per atom, as a function of strain for the different cases.

## V. CORRELATION FUNCTION

An additional way to gain insight into the localization process is to look at the spatial correlations of  $D_{ave}^2$  using a correlation function. This is straightforward, since by choosing a regular array of boxes in which to average, we get  $D_{ave}^2$  defined on a lattice. We define the correlation function  $C_D(\Delta)$ , where  $\Delta$  is a two-dimensional integer difference vector, by

$$C_D(\Delta) \equiv \frac{\langle D_{ave}^2(\mathbf{a})D_{ave}^2(\mathbf{a} + \Delta) \rangle - \langle D_{ave}^2 \rangle^2}{\langle (D_{ave}^2)^2 \rangle - \langle D_{ave}^2 \rangle^2}, \quad (1)$$

where  $\mathbf{a} \equiv (i, j)$  represents an arbitrary lattice point and angle brackets denote averages over  $\mathbf{a}$ , for a particular configuration. The normalization is chosen so that the function is unity at the origin. Although the lattices for different configurations in a simulation are not equivalent, the lattice constant (the size of the boxes in which  $D_{ave}^2$  is calculated) is nearly the same for each configuration, about 2.5 nm.<sup>48</sup> This means that it is allowable to average  $C_D$ 's from different configurations if we restrict  $\Delta$  to a common range ( $|\Delta|$  can be up to half the system size). In some cases such averaging is useful to create a smoother image.

Figure 10 shows contour plots of  $C_D$  averaged over configurations between 5% and 10% strain, and 10% and 15% strain, in the  $56 \times 56 \times 1.8$  nm system with a notch, deformed at the faster strain rate. In all contour plots shown, the contour values are separated by 0.1, and the zero contour is highlighted in white. The function has a characteristic four-fold symmetry, with positive correlation at  $45^\circ$  angles. This is consistent with the existence of two shear bands, each leaving the notch at  $45^\circ$  in opposite directions. In the former case  $C_D$  has some extra roughness, and the four-fold pattern extends only a little away from the center, which is consistent with the fact that the shear bands have not yet fully developed. In the latter, the pattern is stronger, consistent with shear bands having fully developed. Figure 11 shows the correlation function for the same system deformed at the

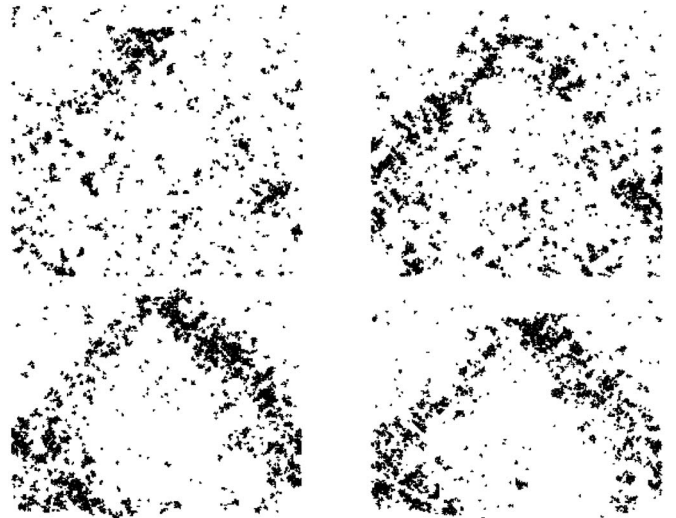


FIG. 9. Visualization using  $D_{min}^2$  in sample D deformed at the slower strain rate, at 4%, 5%, 10%, and 15% strain. At this strain rate the shear bands are already well developed at 5% strain. They also appear to be more intense, particularly the one on the right.

slower strain rate at 5% and 10% strain. At this strain rate, there is already strong diagonal correlation at 5%, particularly in the  $y=-x$  direction, corresponding to the more intense shear band on the right that was noted earlier. At 5% the difference is not so large, but it is very clear at 10% strain, where even at the edges of the image in the  $y=-x$  direction, at a distance of 10 nm, the correlation still has a value greater than 0.4.

It is interesting to look at  $C_D$  from a simulation with no notch (sample C), where no clear shear bands have formed. Initially the correlation is quite weak, and lacking the characteristic four-fold pattern, but by 25%–30% strain, however, a smoother pattern emerges, Fig. 12, with correlation favored particularly on one of the diagonals, the line  $y=x$ . Looking at a visualization of the system at 25% strain, the lower part of Fig. 12, two weak bands can be discerned with directions parallel to the line  $y=x$ . Again this shows the usefulness of  $C_D$  in providing an accurate picture of the spatial heterogeneity—the bands are far from obvious without having  $C_D$  as a guide.

If we now look at the system without a notch deformed at the slower strain rate, we see some interesting behavior.

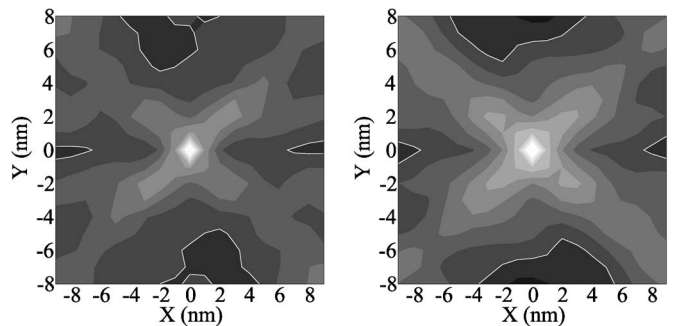


FIG. 10. Lattice correlation function  $C_D$  from sample D, at the faster strain rate. Left, averaged between 5% and 10% strain; right, averaged between 10% and 15% strain.

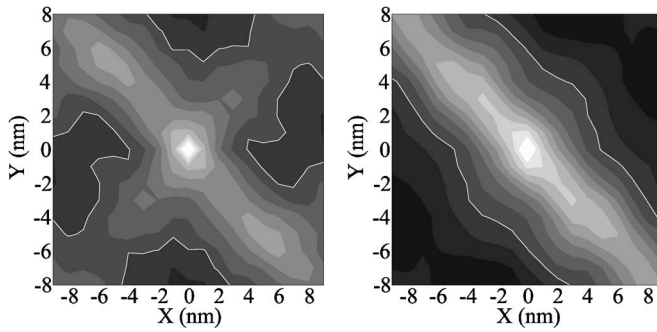


FIG. 11. Lattice correlation function for  $D_{ave}^2$  from sample D, the slower strain rate, at 5% and 10% strain. It is clear that the shear band on the right of the sample, parallel to the line  $y=-x$ , is significantly more intense.

First, looking at the visualization of  $D_{min}^2$  in Fig. 13, it is clear that two shear bands at  $45^\circ$  have formed by 10% strain. It is fortuitous that the bands lie at the same locations as in the simulations with a notch. In fact, the consideration of visualizations of the entire deformation history indicates that the initial intersection of the bands is not at the sample edge, but about one-quarter of the sample width from it. The intersection then moves toward the edge, suggesting that it is somehow favorable to have the intersection at the edge. In the lower part of Fig. 13 are shown contour plots of the correlation function corresponding roughly to the same stages of deformation. The evolution toward a state with well-defined shear bands is clear.

## VI. TEMPERATURE RISE

A recurring question in the study of shear bands has been whether a significant temperature rise takes place inside a shear band. Evidence for this includes the vein pattern on fracture surfaces, which suggests local melting. On the other hand, attempts to infer a temperature rise from the amount of plastic strain in the band suggest rises between a few and 100 K,<sup>29,30</sup> but definitely below the glass transition temperature. In order to check for local heating we again make a coarse graining onto a lattice. This time the quantity averaged in a given box is the kinetic energy per atom, normalized to give a temperature in Kelvin.<sup>49</sup> There are typically about 500 atoms in each box, which provide enough self-averaging that time averaging is not needed to give a meaningful temperature. An example of this is shown in Fig. 14, and it shows clearly an increase of temperature along the shear bands, of order 25 K at this point (colors indicate temperature intervals of width 25 K); the temperature difference between the hottest and coolest parts of the system is of order 50 K, and reaches 100 K at larger strains. Upon examining the whole process (most easily by making an animation), it is clear that, initially, increases of temperature start at the notch itself (this can be seen happening with the area of yellow near the notch, indicating 150 K) and propagate along the bands. Subsequently, the zone of intersection of the bands, and their intersection with the free surface on the far side of the sample, also act as “hot spots,” initiating further increases in temperature.

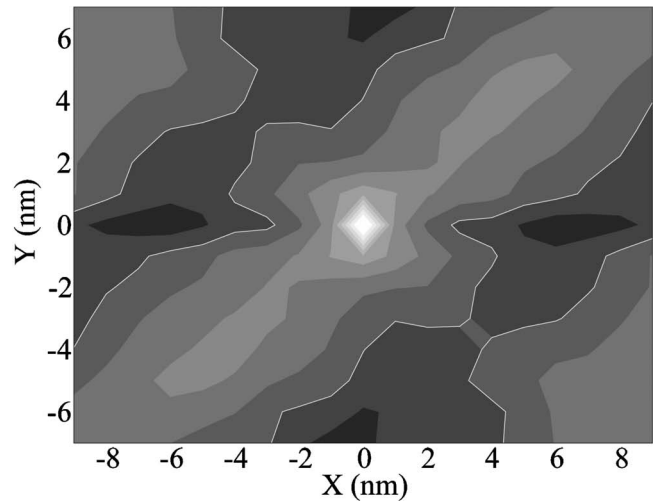


FIG. 12. Above, the lattice correlation function for  $D_{ave}^2$  from sample C, the faster strain rate, averaged between 25% and 30% strain. Below, visualization using  $D_{min}^2$  at 25% strain. The emergence of shear bands parallel to  $y=x$  is clear in the first case and discernible in the second.

Figures 15 and 16 and show the temperature rises for the slower strain rate, and for the faster strain rate without a thermostat, respectively. At the slower strain rate and with a thermostat, a distinct feature is the asymmetry between the two bands; only the one oriented along  $y=-x$  seems to have a raised temperature. This is consistent with the asymmetry found in  $C_D$  previously. With no thermostat, the region of raised temperature again starts in the shear bands and spreads over the whole system, and the temperature difference between the hottest and coolest parts of the system reaches again about 100 K. The width of the temperature peak can be obtained by plotting temperature profiles as we did for  $D_{ave}^2$  (not shown) and is close to 12 nm in all cases, or slightly more than the width of the  $D_{ave}^2$  profiles.

To investigate the causal relationship between shear localization and local heating we show in Fig. 17 the maximum values of the temperature and  $D_{ave}^2$  peaks as a function of strain for the notched  $56 \times 56 \times 1.8$  nm system at the faster strain rate. As we have seen, the  $D_{ave}^2$  localization occurs over the interval 5%–10% strain. Here we also see that the temperature rise is somewhat delayed—it does not start until just before 10% strain, whereupon there is a rapid rise of order 10 K, which gives over to a more gradual, steady increase. In the inset is shown the same for the slower strain rate. Here the rise in  $D_{ave}^2$  is even more rapid as a function of

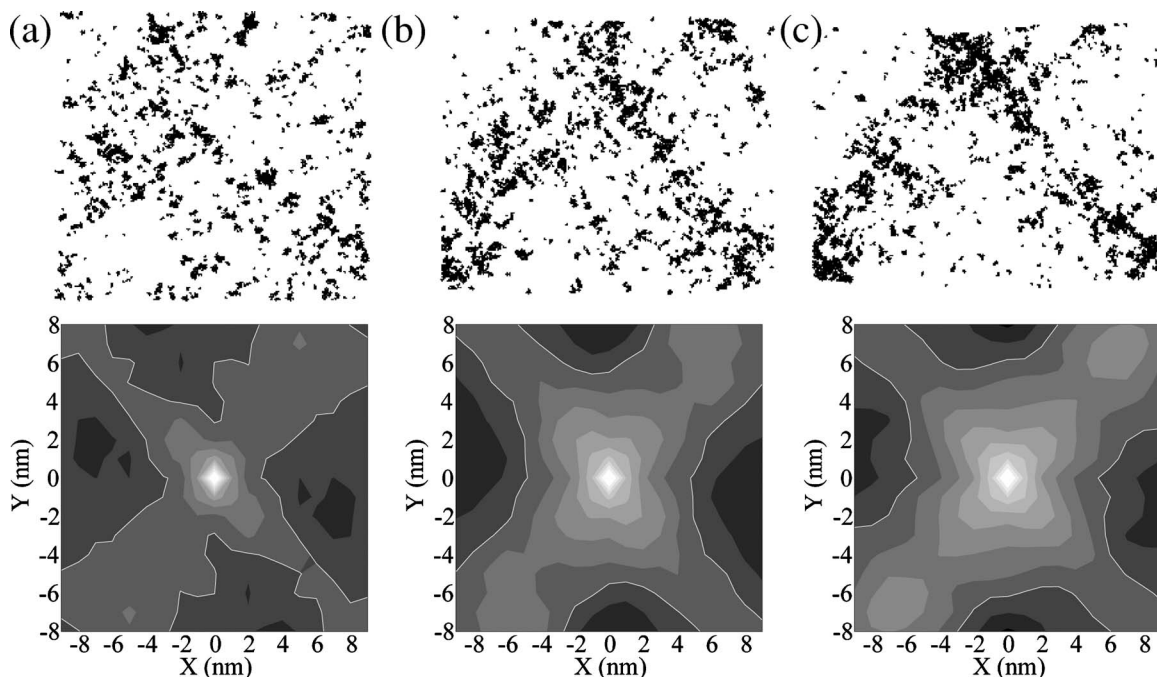


FIG. 13. Above, the visualization of  $D_{min}^2$  in sample C deformed at the slower strain rate at (a) 5% (b) 10%, and (c) 15% strain. Below, the correlation function averaged over 5—7.5%, 10—12.5%, and 15—17.5%. There is clearly an evolution toward a state with well-defined shear bands.

strain, while the temperature rise is even more gradual. We can conclude, as Wright *et al.* have done,<sup>29,30</sup> that the temperature rise is not a cause of strain localization; rather it must be the other way around.

As mentioned above, as well as the initial notch, extra heating seems also to initiate on the bottom edge, coinciding with the intersection of the shear bands, not only with the free surface, but also with each other. To show that both of these interactions are relevant, we have done simulations on a sample (G) that is twice as long in the  $x$  direction, so that the bands cannot interact with each other and one (H) that is twice is long in the  $y$  direction so that the bands interact with each other away from the free surfaces. Figures 18 and 19 show the temperature plots for these at 25% and 35% strain, respectively. It is clear that local heating is enhanced by both types of interactions: shear band-shear band and shear band-surface, although the latter seems to be the stronger effect, since the temperature rise in Fig. 19 is still only 25 K at most, even though the amount of deformation is greater.

## VII. DENSITY CHANGES

As has been mentioned, it still is largely unclear what leads to the contrast in TEM measurements—how are the shear bands at all visible? Some, but not all, of the contrast is due to changes in thickness of the sample, since deformed regions tend to have less resistance of chemical attack during thinning.<sup>19,31</sup> Even if this explains the contrast, there is still clearly some structural difference between the shear bands and their surroundings. An obvious possibility is simply a change in density in the bands. One expects this to decrease, corresponding to an increase in the so-called free volume,

which is the basis for various theories of deformation in amorphous systems that involve the creation of free volume during deformation.<sup>32–34</sup> While the notion of free volume as a direct mediator of atomic rearrangements is no longer taken literally, it is nevertheless natural to expect a decrease in density in regions that have been substantially deformed. This is because there is a clear inverse correlation between the enthalpy and the density, and one expects the enthalpy to be locally increased (which can be called disordering, even if the actual structural changes are not obvious), during deformation. The TEM work of Donovan and Stobbs<sup>19</sup> indicated that dilation occurred in the shear bands in both compression and tension, with voids forming in samples deformed in tension. The volume increase inferred by them is of order 10%, which is surprisingly large. Other authors<sup>31,35</sup> have reported evidence for nm-sized voids forming (also in tension) based on Fourier analysis of TEM micrographs. These are presumed to have formed by a “condensation” of excess free volume generated during deformation.

We can calculate the local density in the simulations, similarly to the local temperature—by dividing the system into boxes of a given volume and counting the atoms in each box. Figure 20 shows plots of this local density for a notched system deformed at the slower strain rate at zero strain, and 20% strain, and with two different box sizes for coarse graining. The first noticeable feature is that, at a coarse-grain length of 2.5 nm at least, the intrinsic fluctuations are at least comparable to any systematic change within the shear bands. This could probably be improved with a little averaging over time so that fluctuations due to atoms being very close to the box sides could be smoothed. With 7.5 nm coarse graining, there appears to be an effect in that the regions of lowest density, colored red, lie within the shear bands, although they

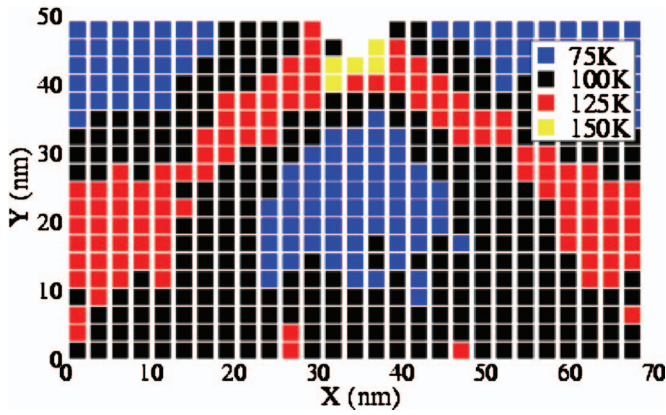


FIG. 14. (Color) Temperature plot of sample D deformed at the faster strain rate at 100 K, at 20% strain. Each square is 2.5 nm  $\times$  2.5 nm. The temperature is seen to be increased around the shear bands.

do not extend the whole length of the bands. The difference between these regions and the surrounding (orange and orange-yellow) regions is of order 1%. This is much lower than the figure reported by Donovan and Stobbs, but it seems reasonable. Note that this change is an order of magnitude greater than would be expected due solely to the temperature increase, assuming a typical value of the volume coefficient of thermal expansion<sup>36</sup> to be around  $5 \times 10^{-5} \text{ K}^{-1}$  and noting that the temperature rise at this strain is no more than 25 K (Fig. 15).

VIII. DISCUSSION

Despite a wealth of experimental data, there is much that is not understood about shear bands. This not only includes why they form in the first place, but also what determines their width, what distinguishes them structurally from the surrounding material, how high the temperature actually gets inside an active shear band, etc. Beyond the properties of individual shear bands, there are questions regarding their interactions with each other, with free surfaces, and with

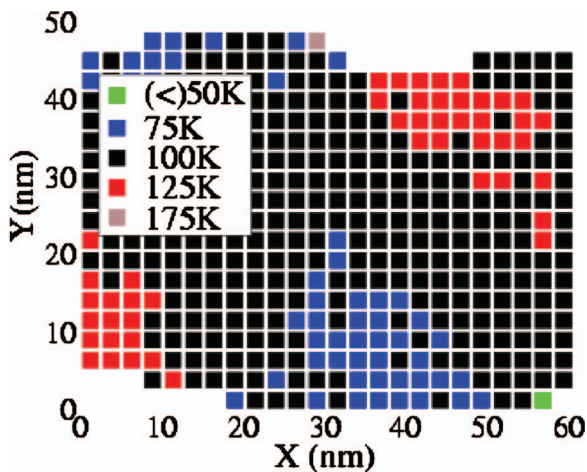


FIG. 15. (Color) Temperature plot of sample D deformed at the slower strain rate at 100 K, at 30% strain.

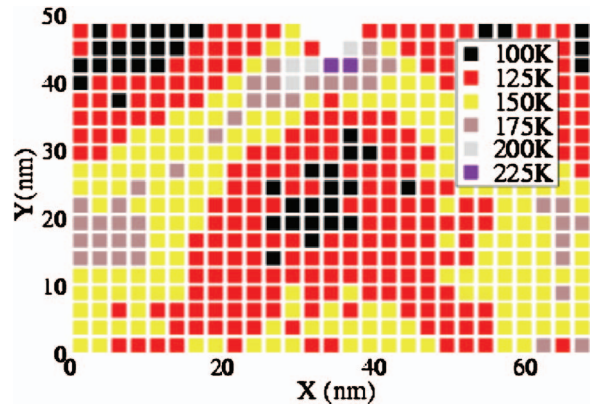


FIG. 16. (Color) Temperature plot of a sample D deformed at the faster strain rate with thermostat turned off after equilibration to 100 K, 20% strain.

crystals. Many of these issues can be addressed by atomistic simulation since the length scale associated with a shear band, 10 nm or so, is well within the current computational capability.

In this work we have sought to characterize shear bands in a realistic model glass in a detailed manner. We have chosen the simulation geometry carefully to allow the straightforward generation of shear bands during deformation. Defining shear bands in terms of atoms whose environments are undergoing nonaffine transformations, we have calculated their width to be on the order of 10 nm, and their formation time to be of the order of tens of picoseconds. There seems to be a reduction in density within an active shear band of, at most, 1%. Our data is not sufficient to identify a propagation speed of the shear bands; this would probably require larger simulations in all three directions: in the plane so that the time to propagate across the sample exceeds the formation time, allowing a reliable speed estimate, and out of the plane to get smoother  $D_{ave}^2$  profiles, which would allow a more accurate determination of the “front” of the shear band. The temperature rise within shear bands has been shown to be a conse-

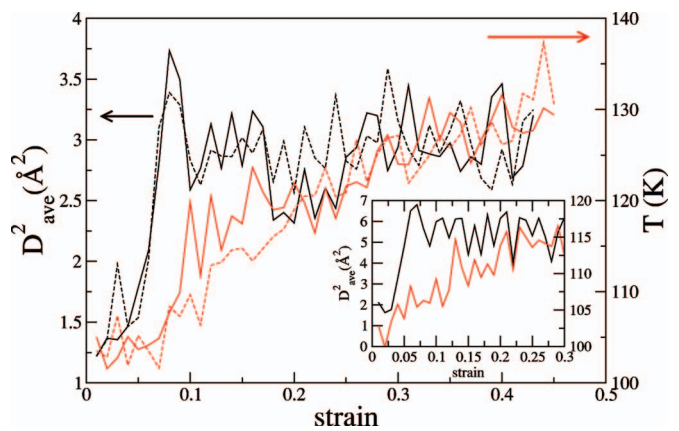


FIG. 17. (Color) Peak heights of profiles of  $D_{ave}^2$  (black) and temperature (red) for sample D deformed at the faster strain rate. Solid and dotted lines denote profiles at  $y' = -20 \text{ nm}$  and  $-30 \text{ nm}$ , respectively. Inset: the same for the slower strain rate,  $y' = -20 \text{ nm}$ . It is seen that  $D_{ave}^2$  rises first, and then temperature.

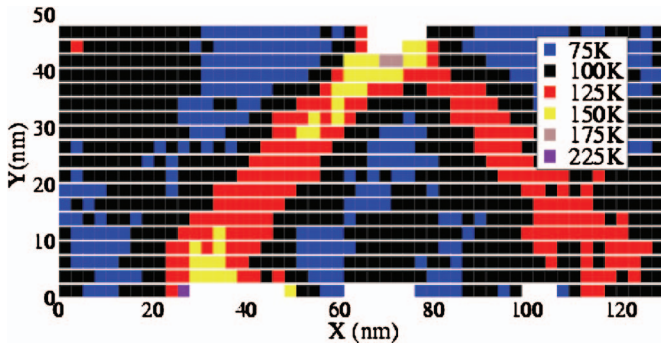


FIG. 18. (Color) Temperature plot of sample G deformed at the faster strain rate at 100 K, 25% strain. The temperature rise is seen to be larger, where the shear bands meet the surface, particularly on the left.

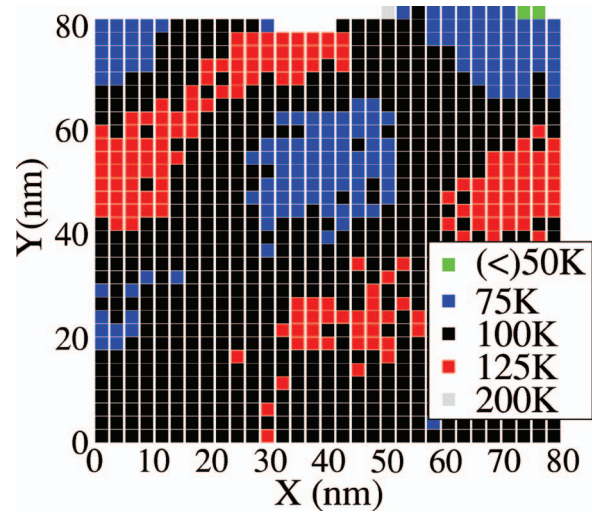


FIG. 19. (Color) Temperature plot of sample H deformed at the faster strain rate at 35% strain. The temperature rise is increased where the shear bands intersect.

quence rather than a cause of the localization, which is consistent with some recent experimental studies.

The correlation function of  $D_{ave}^2$  has been found useful for identifying localization that is not apparent simply by visualizing the atoms. It is interesting that even when there appears to be only one band, as in Fig. 12, there is still some correlation also apparent on the opposite diagonal, suggesting an underlying tendency toward a four-fold symmetric correlation. This is highly reminiscent of the stress change that occurs in a strained elastic medium due to a localized plastic slip event that can be expressed<sup>37</sup> in terms of a Green's function of the form  $G(r, \theta) = \cos(4\theta)/r^2$ . This has been used in lattice models of deformation of amorphous

materials,<sup>38,39</sup> while Langer<sup>40</sup> has attempted to incorporate the spatial dependence of the effect of local plasticity into the Shear Transformation Zone (STZ) theory. Of particular interest in such theories would be an understanding of how the shear bandwidth is determined by the characteristics of these “elementary events,” such as how their activation depends on stress, or on the degree of annealing of the system, whether some kind of screening plays a role, etc.

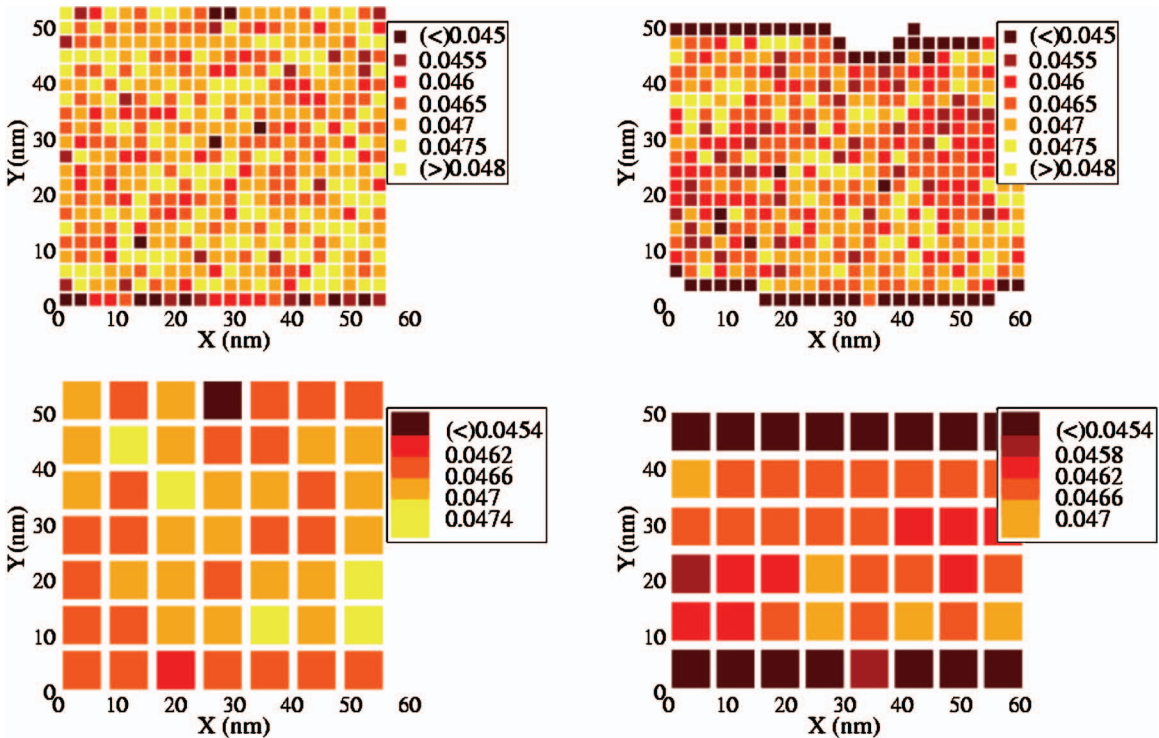


FIG. 20. (Color) Density plots of sample D deformed at strain rate S. The coarse-graining length is 2.5 nm in the upper plots and 7.5 nm in the lower ones. The plots on the left are for the undeformed system, while those on the right are at 20% strain. Dark squares at the edge are typically boxes that are only partially filled with atoms. A reduction of density in the areas associated with shear bands is apparent in the right figures.

A frequently raised issue in simulations of amorphous metals is the degree of annealing of the sample, or alternatively the appearance of aging and rejuvenation phenomena. Aging refers to the time dependence of calculated quantities (potential energy, relaxation time) that is due to the system being out of equilibrium and therefore approaching equilibrium; the potential energy tends to relax downward. Straining the system, particularly at high strain rates, undoes this effect, leading to higher-energy states (even after the stress is removed); these effects, being the opposite of aging, are thus known as rejuvenation effects.<sup>41,42</sup> Shi and Falk, simulating uniaxial deformation<sup>9</sup> and nanoindentation,<sup>43</sup> have recently shown the influence of the cooling rate on the tendency for shear bands to develop; slower cooling makes them more likely. If we compare our cooling rates to theirs by expressing them in units of  $T_g/t_0$ , where  $t_0$  is a time scale constructed from the basic energy, length, and mass scales—here we choose it to be 0.3 ps—then the cooling rate we have used in these simulations is  $R=7.2 \times 10^{-4} T_g/t_0$ , which corresponds to the fastest cooling rate used by Shi and Falk (not including the instantaneous quenches), and differs from their slowest rate by a factor of order 500. This would suggest that our samples are not particularly optimal for the formation of shear bands, although there were possibly significant differences between our material and theirs; in particular, their material is strictly two dimensional and they have used a pair potential (Lennard-Jones) to describe interactions.

In our work simulating homogeneous deformation in pure shear<sup>44</sup> we have noted that the largest effect of variations in cooling rate appears to be the height of the initial peak. The flow stress is more or less independent of the cooling rate, while the potential energy of a better-cooled system starts off, naturally, lower than that of a less well-cooled system, but approaches it during the flow regime due to rejuvenation effects. This is consistent with the findings of Varnik and co-workers.<sup>7</sup> A more direct sign of aging is observed if the strain rate is slow compared to the cooling rate; in this case, upon applying strain, the potential energy is seen to initially decrease, before increasing due to the elastic energy. This is seen to a very small extent in our simulations at the slower strain rate, where the energy goes down by less than 0.1 meV per atom between zero and 0.2% strain before rising again. This is not an important effect.

The shear bands we see at the higher strain rate do not form until somewhat after the stress peak, which, based on our previous work, would suggest that they could be relatively immune to variations in the cooling rate, but at the slower strain rate they form already at 5% strain, right around the stress peak, and thus could well be affected by the cooling rate. The shear bands described by Shi and Falk<sup>9</sup> were formed also by 5% strain. We are in the process of creating more slowly cooled samples. It will be interesting to explore the effects of both cooling and strain rate on the characteristics of shear bands that have been presented here. It should be pointed out, however, that for the foreseeable future, simulations will continue to be relatively fast and cannot capture long-time processes. Structural relaxation

processes taking place on the microsecond time scale have been observed already in computer simulations with less than  $10^3$  atoms;<sup>45,46</sup> such time scales can hardly be reached with the system sizes used here, so we must concede that not all relevant processes are accessible. This would possibly still be true even if microsecond time scales were within reach—it is quite possible that different processes take place on even longer time scales, but still shorter than the experimental ones.

Considering size limitations now, we have noted that the intersection of the bands seems to cause little change in the stress-strain curve; on the other hand, there can presumably also be interactions even when there is no intersection, and thus we cannot rule out the possibility of the observed shear band behavior being influenced by such interactions. Larger systems would be useful in this regard. Ideally one would have a simulation with just one shear band; this has been achieved in simulations with walls,<sup>7</sup> but then one can probably not exclude effects due to the interaction between the band and the wall(s).

The task of studying the properties of individual shear bands is analogous to studying the properties of individual dislocations in crystalline materials. The deformation of metallic glasses often involves interacting shear bands and other complicated processes, as evidenced by the complex vein patterns on fracture surfaces where the feature size is of order one micron, i.e., mesoscopic in scale. Clearly, a complete understanding of the deformation of metallic glasses will require theory and modeling at the mesoscopic scale, which require an understanding of processes at the microscopic scale. The work presented here is a step toward providing such a basic understanding. Important questions regarding the basic physics of the phenomena presented here remain open: How do elementary slip processes lead to the shear band formation? What determines the shear bandwidth? Possibly related to the last question is the observation of the scaling of event sizes by Maloney and Lemaître in zero-temperature simulations of two-dimensional materials.<sup>47</sup> Here the systems are small enough that individual events can be resolved. Their size, characterized in terms of either an energy drop or a stress drop, is seen to scale with the linear system size  $L$ . We are currently investigating this behavior in the present, three-dimensional system. The lengths over which this scaling has been observed are only a few nm. It is clear that, at finite temperature, scaling must break down at some length scale. One might speculate that this would be the length scale at which mesoscopic heterogeneities, such as the shear bands reported here, occur. Clearly, further work is needed to make such a connection.

#### ACKNOWLEDGMENTS

This work was supported by the EU Network on bulk metallic glass composites (MRTN-CT-2003-504692 “Ductile BMG Composites”) and by the Danish Center for Scientific Computing through Grant No. HDW-1101-05. Center for Individual Nanoparticle Functionality (CINF) is sponsored by The Danish National Research Foundation.

\*Electronic address: nbailey@fysik.dtu.dk

- <sup>1</sup>A. L. Greer, *Science* **267**, 1947 (1995).
- <sup>2</sup>W. L. Johnson, *MRS Bull.* **24**, 42 (1999).
- <sup>3</sup>W. L. Johnson, *JOM* **54**, 40 (2002).
- <sup>4</sup>J. Schroers and W. L. Johnson, *Phys. Rev. Lett.* **93**, 255506 (2004).
- <sup>5</sup>J. Das, M. B. Tang, K. B. Kim, R. Theissmann, F. Baier, W. H. Wang, and J. Eckert, *Phys. Rev. Lett.* **94**, 205501 (2005).
- <sup>6</sup>C. C. Hays, C. P. Kim, and W. L. Johnson, *Phys. Rev. Lett.* **84**, 2901 (2000).
- <sup>7</sup>F. Varnik, L. Bocquet, J.-L. Barrat, and L. Berthier, *Phys. Rev. Lett.* **90**, 095702 (2003).
- <sup>8</sup>M. L. Falk and Y. Shi, *Mater. Res. Soc. Symp. Proc.* **754**, 257 (2003).
- <sup>9</sup>Y. Shi and M. L. Falk, *Phys. Rev. Lett.* **95**, 095502 (2005).
- <sup>10</sup>D. Deng, A. S. Argon, and S. Yip, *Philos. Trans. R. Soc. London, Ser. A* **329**, 613 (1989).
- <sup>11</sup>S. M. Foiles, M. I. Baskes, and M. S. Daw, *Phys. Rev. B* **33**, 7983 (1986).
- <sup>12</sup>K. W. Jacobsen, *Comments Condens. Matter Phys.* **14**, 129 (1988).
- <sup>13</sup>M. L. Falk and J. S. Langer, *Phys. Rev. E* **57**, 7192 (1998).
- <sup>14</sup>D. L. Malandro and D. J. Lacks, *J. Chem. Phys.* **110**, 4593 (1999).
- <sup>15</sup>X. K. Xi, D. Q. Zhao, M. X. Pan, W. H. Wang, Y. Wu, and J. J. Lewandowski, *Phys. Rev. Lett.* **94**, 125510 (2005).
- <sup>16</sup>F. Abraham, R. Walkup, H. Gao, M. Duchaineau, T. Diaz de la Rubia, and M. Seager, *Proc. Natl. Acad. Sci. U.S.A.* **99**, 5783 (2002).
- <sup>17</sup>C. L. Rountree, R. K. Kalia, E. Lidorikis, A. Nakano, L. Van Brutzel, and P. Vashishta, *Annu. Rev. Mater. Res.* **32**, 377 (2002).
- <sup>18</sup>J. Schiøtz and K. W. Jacobsen, *Science* **301**, 1354 (2003).
- <sup>19</sup>P. E. Donovan and W. M. Stobbs, *Acta Metall.* **29**, 1419 (1981).
- <sup>20</sup>E. Pekarskaya, C. P. Kim, and W. L. Johnson, *J. Mater. Res.* **16**, 2513 (2001).
- <sup>21</sup>P. H. Mott, A. S. Argon, and U. W. Suter, *Philos. Mag. A* **67**, 931 (1993).
- <sup>22</sup>F. Sommer, G. Bucher, and B. Predal, *J. Phys. Colloq.* **41**, 563 (1980).
- <sup>23</sup>A. Inoue, A. Kato, T. Zhang, S. G. Kim, and T. Masumoto, *Mater. Trans., JIM* **32**, 609 (1991).
- <sup>24</sup>K. W. Jacobsen, P. Stoltze, and J. K. Nørskov, *Surf. Sci.* **366**, 394 (1996).
- <sup>25</sup>N. P. Bailey, J. Schiøtz, and K. W. Jacobsen, *Phys. Rev. B* **69**, 144205 (2004).
- <sup>26</sup>J. J. Lewandowski, W. H. Wang, and A. L. Greer, *Philos. Mag. Lett.* **85**, 77 (2005).
- <sup>27</sup>M. P. Allen and D. J. Tildesley, *Computer Simulation of Liquids* (Oxford University Press, 1987).
- <sup>28</sup>T. Shimokawa, A. Nakatani, and H. Kitagawa, *Phys. Rev. B* **71**, 224110 (2005).
- <sup>29</sup>W. J. Wright, R. B. Schwarz, and W. D. Nix, *Mater. Sci. Eng., A* **319-321**, 229 (2001).
- <sup>30</sup>W. J. Wright, R. Saha, and W. D. Nix, *Mater. Trans., JIM* **42**, 642 (2001).
- <sup>31</sup>W. H. Jiang and M. Atzmon, *Acta Mater.* **51**, 4095 (2003).
- <sup>32</sup>F. Spaepen, *Acta Metall.* **25**, 407 (1977).
- <sup>33</sup>P. S. Steif, F. Spaepen, and J. W. Hutchinson, *Acta Metall.* **30**, 447 (1981).
- <sup>34</sup>W. L. Johnson, J. J. Lu, and M. D. Demetriou, *Intermetallics* **10**, 1039 (2002).
- <sup>35</sup>J. Li, Z. L. Wang, and T. C. Hufnagel, *Phys. Rev. B* **65**, 144201 (2002).
- <sup>36</sup>A. R. Yavari, A. Le Moulec, A. Inoue, N. Nishiyama, N. Lupu, E. Matsubara, W. J. Botta, G. Vaughan, M. Di Michiel, and A. Kvik, *Acta Mater.* **53**, 1611 (2005).
- <sup>37</sup>G. Picard, A. Ajdari, F. Lequeux, and L. Bocquet, *Eur. Phys. J. E* **15**, 371 (2004).
- <sup>38</sup>J.-C. Baret, D. Vandembroucq, and S. Roux, *Phys. Rev. Lett.* **89**, 195506 (2002).
- <sup>39</sup>G. Picard, A. Ajdari, F. Lequeux, and L. Bocquet, *Phys. Rev. E* **71**, 010501(R) (2005).
- <sup>40</sup>J. S. Langer, *Phys. Rev. E* **64**, 011504 (2001).
- <sup>41</sup>M. Utz, P. G. Debenedetti, and F. H. Stillinger, *Phys. Rev. Lett.* **84**, 1471 (2000).
- <sup>42</sup>D. J. Lacks and M. J. Osborne, *Phys. Rev. Lett.* **93**, 255501 (2004).
- <sup>43</sup>Y. Shi and M. L. Falk, *Appl. Phys. Lett.* **86**, 011914 (2005).
- <sup>44</sup>N. P. Bailey, J. Schiøtz, and K. W. Jacobsen (unpublished).
- <sup>45</sup>H. Teichler, *J. Non-Cryst. Solids* **293-295**, 339 (2001).
- <sup>46</sup>H. Teichler, *Phys. Rev. E* **71**, 031505 (2005).
- <sup>47</sup>C. Maloney and A. Lemaître, *Phys. Rev. Lett.* **93**, 016001 (2004).
- <sup>48</sup>This is the nominal value, which is altered slightly to allow an integer number of boxes to fit in each direction of the system. Also the box size in the  $z$  direction is chosen to be the height of the simulation cell, so that there is only one layer of boxes, and thus the subsequent analysis is entirely two-dimensional.
- <sup>49</sup>The kinetic energy used here, unlike that used by the dynamics, includes velocity contributions from the strain rate, which could cause an apparent temperature gradient along the sample, but the magnitude of this is expected to be of order 10 K, which is less than the resolution of the temperature plots.